J Fluoresc (2015) 25:1481–1492
DOI 10.1007/s10895-015-1639-5

ORIGINAL ARTICLE

Synthesis, Characterization, Fluorescence, Photocatalytic and Antibacterial Activity of CdS Nanoparticles Using Schiff Base

Dasari Ayodhya[1] · M. Venkatesham[1] · A. Santoshi Kumari[1] · G. Bhagavanth Reddy[1] · D. Ramakrishna[1] · G. Veerabhadram[1]

Received: 28 April 2015 / Accepted: 3 August 2015 / Published online: 15 August 2015
© Springer Science+Business Media New York 2015

Abstract Cadmium sulfide nanoparticles (CdS NPs) were successfully prepared using sonochemical method by employing Schiff-base, (2-[(4-methoxy-phenylimino)-methyl]-4-nitro phenol) as a complexing agent. Here, SB is used as a ligand to control the morphology of NPs. XRD patterns and TEM images show that the synthesized CdS NPs have cubic structures with a diameter of about 2–10 nm. The formation of CdS NPs and their optical, structure, thermal and morphologies were studied by means of UV-vis DRS, fluorescence, FTIR, zeta potential, XRD, SEM and TEM. The interactions between CdS NPs and SB were investigated in an aqueous solution using fluorescence spectroscopy. The fluorescence quenching studies suggest that SB quenches the fluorescence of CdS NPs effectively. The degradation kinetics of methyl red (MR) by the photocatalyst was followed by Langmuir-Hinshelwood model. The results revealed that photocatalytic degradation of MR by SB capped CdS NPs could be considered as a practical and reliable technique for the removal of environmental pollutants. The antibacterial activity of samples was evaluated against *E. coli, S. aureus and P. aeruginosa* and the results were compared. SB and SB capped CdS NPs could be a potential antibacterial compounds after further investigation.

Keywords CdS nanoparticles · Schiff base · Fluorescence studies · Photodegradation · Antibacterial activity

✉ G. Veerabhadram
gvbhadram@gmail.com

[1] Department of Chemistry, Osmania University, Hyderabad, Telangana State 500007, India

Introduction

Among the chalcogenide compounds belonging to the II–VI family, CdS has received much attention due to the fact that it has a wide band gap of 2.42 eV at room temperature. It possesses many excellent physical and chemical properties which have promising applications in multiple technical fields including lasers, light-emitting diodes, sensors, solar cells and in photochemical catalysis [1–6]. Several methods have been explored towards the synthesis of CdS NPs, such as microwave-solvothermal method, [7] sonochemical method [8] and the surfactant–ligand co-assisting solvothermal method [9]. The methods listed above are in vogue to control the size and growth of CdS nanostructures. These are done by using coating agents, such as surfactants, ligands or polymers to limit the growth of the nanomaterial structure. In recent years, sonochemical methods have been greatly investigated to prepare different nanostructures, including rods [10], wires [11], tubes [12], particles [13], and porous spheres [14]. During sonochemical method, ultrasonic sound wave radiations cause short required time and low temperature to carry out chemical reaction. The sound wave radiations are beneficial to the morphology and size of the samples, too.

Most dyes, used in the pigmentation of textiles, paper, leather, ceramics, cosmetics and food-processing products, are derived from azo dyes. These are characterised by the presence of one or more azo groups (-N = N-) in their structure [15]. Approximately 15 % of the dyes produced worldwide are lost within waste water during synthesis and processing [16]. This waste represents an enormous hazard to human and environmental health due to the toxicity of azo dyes [17]. Removal of the colour of dyes and complete mineralization of C, N and S hetero atoms into CO_2, NH_4^+, NO_3^- and SO_4^{2-}, respectively has also been studied by them. Rajeshwar et al. [18] focused on the heterogeneous photocatalytic treatment of

organic dyes present in air and water. They have used TiO_2, ZnO, CdS, WO_3 and Fe_2O_3 for decolorizing and decomposing the organic dye to mineralized products. UV spectrophotometry was used to measure the bleaching efficiency. The mineralization efficiency was calculated from total organic carbon (TOC) measurements. Herrmann et al. reported, in the MR degradation, TOC elimination is fastest and most easy [19]. The CdS NPs suspension prepared in this study has an extremely strong adsorption towards MR. Although pH_{ZPC} for MR is estimated to be 5.4, it was found that repulsive electrostatic interactions between the CdS surface play an important role. Guindo et al. [20] reported even lower values of pHzpc between 1 and 1.5 for spherical CdS particles prepared by the method of Matijevic and Wilhemy [21]. At pH higher than pH_{ZPC} (for CdS), as the photogenerated electrons cannot easily overcome the negative charged surface, the holes may be prevented from reacting with the dye, thus ultimately recombining with the electrons.

The use of semiconductors as fluorescence probes has increased in recent years along with their application in different areas such as medicine, chemistry and engineering. This interest is related to their broad absorption spectra and strong and tunable fluorescence [1, 22–24]. It is important to point out the presence of the amine moieties in some of these structures. We are interested in understanding the interaction between simple amines and NPs in order to correlate possible behaviours in more complex structures. CdS NPs are also fluorescent due to the radiative recombination of the electron–hole pair. These light emitting properties have been among the most studied in quantum dots due to an interest in using them as fluorescent probes in bioimaging [25], as well as sensor applications [26, 27]. Fluorescence quenching refers to any process that decreases the fluorescence intensity of a sample. A variety of molecular interactions can result in quenching.

Schiff bases are considered as a very important class of organic compounds which have wide application in many biological aspects. Some Schiff bases were reported to possess antibacterial, antifungal and antitumor activities [28, 29]. Synthesis and crystal structure of 2-[(4-methoxy-phenyl)iminomethyl]-4-nitrophenol was reported earlier [30]. We report in this paper, the synthesis of CdS NPs by Schiff base using sonochemical bath. The quenching studies have been investigated using fluorescence emission spectroscopy technique. The average particle size of the synthesized sample is about 15 nm as determined by XRD. The photocatalytic activity of the prepared samples was evaluated by the photocatalytic decolouration of MR under sunlight irradiation. The heterogeneous photocatalysis of MR by CdS NPs shows effective degradation by using small amount of catalyst. In addition, the antibacterial activity of CdS NPs was evaluated and the results were compared with SB.

Experimental

Materials

All the chemicals used for synthesis purposes were of AR grade, purchased from Sigma Aldrich chemicals, and for spectral analysis spectral grade solvents were used. Double distilled water was used for preparing solutions. The test strains, *Escherichia coli (E. coli)* gram-negative, *Staphylococcus aureus (S. aureus)* gram-positive bacteria and *Pseudomonas aeruginosa (P. aeruginosa)* were purchased from IMTECH, Chandigarh, India. Yeast extract, tryptophan and bacterial-grade agar–agar were purchased from Hi-media Laboratories, Mumbai, India.

Synthesis of 2-[(4-methoxy-phenyl)iminomethyl] -4-nitrophenol (SB)

The Schiff-base, 2-[(4-methoxy-phenyl)iminomethyl]-4-nitrophenol, ($C_{14}H_{12}N_2O_4$) was synthesized by using p-Anisidine in methanol and this was slowly added to 5-Nitrosalicylaldehyde in methanol as shown in Scheme 1. The mixture was refluxed and stirred for 3 h at room temperature. The completion of the reaction was monitored through TLC for the disappearance of the starting compounds. Then, the solvent was evaporated yielding yellow precipitation of 2-[(4-methoxy-phenylimino)-methyl]-4-nitrophenol. The yield was about 85 %. The solid thus obtained was dried in oven.

Analytical Data of SB

Colour: Yellow, Yield: 85 %, M.P. 162 °C. FTIR (υ, cm^{-1}): 3618 (υ-O-H), 3072 (υ-C-H), 1621 (υ-C = N), 1516 (υ-C = C), 1336 (υ-N-O), 1258 (υ-C-O), 887 (υ-C-N). UV (λ_{max}/nm): 236, 352. ^{1}H-NMR ($CDCl_3$, δ, ppm): 14.8 s 1H, 8.7 s 1H, 8.2–8.4 d 2H, 7.2–7.4 d 2H, 6.9–7.1 m 3H, 3.9 s 3H. ESI-MS: m/z=273.2 (M+1).

Synthesis of CdS NPs

In a typical procedure, 0.035 M of $Cd(CH_3COO)_2.2H_2O$ was mixed with appropriate concentration of $Na_2S.9H_2O$ solution

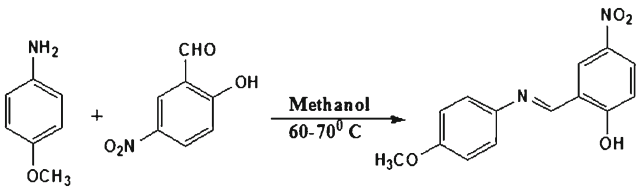

Scheme 1 The synthetic procedure of the formation of SB

under stirring. In a separate beaker, 10^{-3} M of synthesized SB was dissolved in 10 ml DMF. The two solutions were mixed together under stirring and resulting yellow precipitate solution was transferred to a sonochemical bath. After 60 min of sonochemical treatment, the resulting CdS precipitate was collected, filtered, washed with double distilled water and absolute ethanol several times to remove the unreacted chemicals, and finally dried in an oven at 80 °C for 5 h. Similar procedure was adopted to synthesize uncapped CdS NPs.

Characterizations

The morphology of CdS NPs was observed by SEM (scanning electron microscopy, Zeiss evo18) and TEM (transmission electron microscopy, TechnaiG2). Elemental mapping over the selected regions of the CdS NPs was conducted by Energy-dispersive X-ray spectroscopy (EDX). The UV–visible diffuse reflectance spectra (UV-vis DRS) were obtained on the spectrophotometer of Shimadzu UV-3600 equipped with an integrating sphere accessory ($BaSO_4$ was used as a reference). Fluorescence spectra were recorded on a Shimadzu RF-5301PC spectrofluorometer. The FT-IR spectra were recorded on a Shimadzu spectrophotometer. The powder X-ray diffraction (XRD) analysis was made with an X'pert Pro diffractometer. Zeta potential measurements were determined with the Zeta sizer Nano Z (Malvern, UK). ^{1}H-NMR spectra was recorded on Avance-III 400 MHz Fourier Transform Digital NMR Spectrometer at 25 °C (BRUKER BIOSPIN, Switzerland). The Mass spectra were recorded by ESI technique on Shimadzu mass spectrometer.

Fluorescence Measurements

Fluorescence signal was detected in a right angle viewing mode of the incident light and that of emission. Excitation and emission slits were set both at 5.0 nm band-pass. In a typical procedure, the measurement of emission wavelength of SB and SB capped CdS NPs at room temperature. Fluorescence of the mixture was recorded in a quartz cuvette at a fixed excitation wavelength of 350 nm and fluorescence emission wavelengths of SB and SB capped CdS NPs was measured. Subsequently, quenching measurements, the appropriate volume of CdS NPs and a series of SB standard solutions were added to the 10 ml comparison colour tube, diluted by DMF and homogenized for determination. The detection spectra were obtained in the range of 350–650 nm with the excitation wavelength of 350 nm. The whole process was carried out at the room temperature.

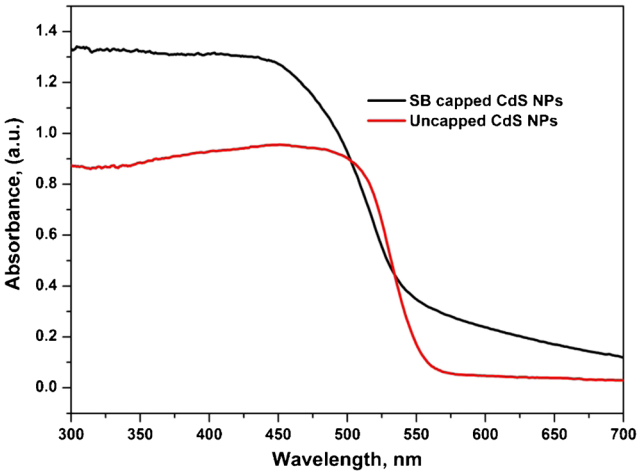

Fig. 1 UV-vis diffuse absorption spectra of CdS NPs

Photocatalytic Activity

The photodegradation of MR solution by varying the amount of CdS NPs was studied. In a typical procedure, 0, 10, 20, 30 and 50 mg amount of the catalyst is added to the 100 ml of the 2×10^{-5} M of MR solution. The reaction suspensions were prepared by adding CdS NPs to the above mentioned MR solution. The suspensions were ultrasonically sonicated for 20 min and stirred in dark for 45 min to ensure an adsorption/desorption equilibrium. The reaction suspensions containing MR and photocatalyst were irradiated by sunlight with continuous stirring. After irradiation the reaction solution aliquots were taken from the reaction solution at regular intervals and centrifuged immediately to remove the catalyst. The absorbance of MR solution was determined at 394 nm (pH=5) for absence and 430 nm (pH=4) for the presence

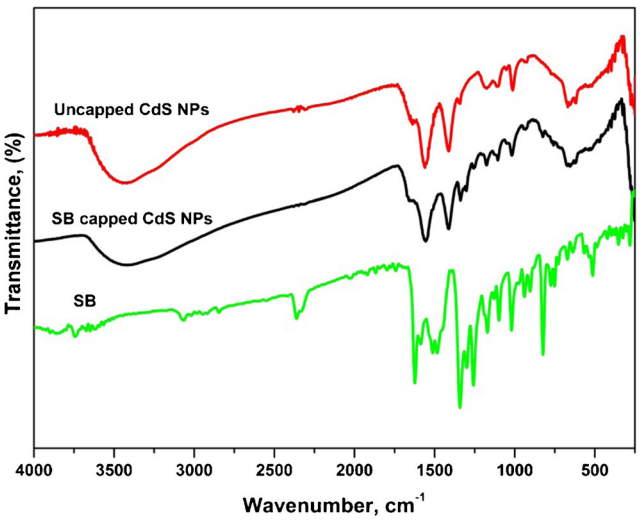

Fig. 2 The FTIR spectrum of CdS NPs

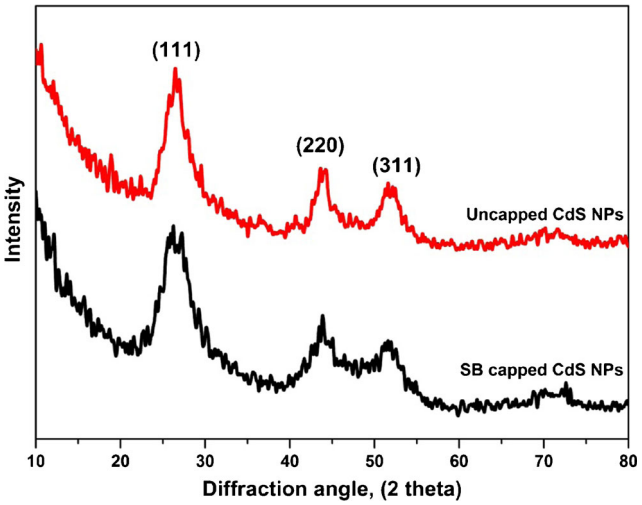

Fig. 3 The XRD spectrum of CdS NPs

of catalyst in photodegradation of MR using an UV-visible spectrophotometer.

Antibacterial Activity

Luria–Bertani (LB) agar medium was prepared by adding yeast extract (0.5 g), tryptophan (1 g), sodium chloride (1 g) and bacterial grade agar (2.5 g) in double distilled water (100 ml). Then the agar medium was sterilized by autoclaving at a pressure of 15 psi and 120 °C temperature for 1 h. This medium was transferred into sterilized Petri dishes in a laminar air flow. After solidification of media, overnight culture of *E. coli* (100 μL), *S. aureus* (100 μL) and *P. aeruginosa* (100 μL) was spread separately on the solid surface of the media. Sterile discs were kept on these inoculated plates with the help of sterile forceps. Sample (10 μL) solutions were placed on these discs and were incubated at 35 °C for 24 h in a bacterial incubator. The inhibition zone that appeared around the disc was measured and recorded as the antibacterial effect of SB, uncapped and SB capped CdS NPs.

Results and Discussion

UV-vis DRS Analysis

UV-vis diffuse absorption edge of CdS NPs is obtained from the plots of absorbance against wavelength. The interception of the tangent on the descending part of the absorption peak of the wavelength axis gives the value of diffuse absorption edge (nm). The UV–vis DRS of uncapped and SB capped CdS NPs were presented in Fig. 1. The absorption peak of CdS NPs can be easily found in the visible region. The wavelength for pure

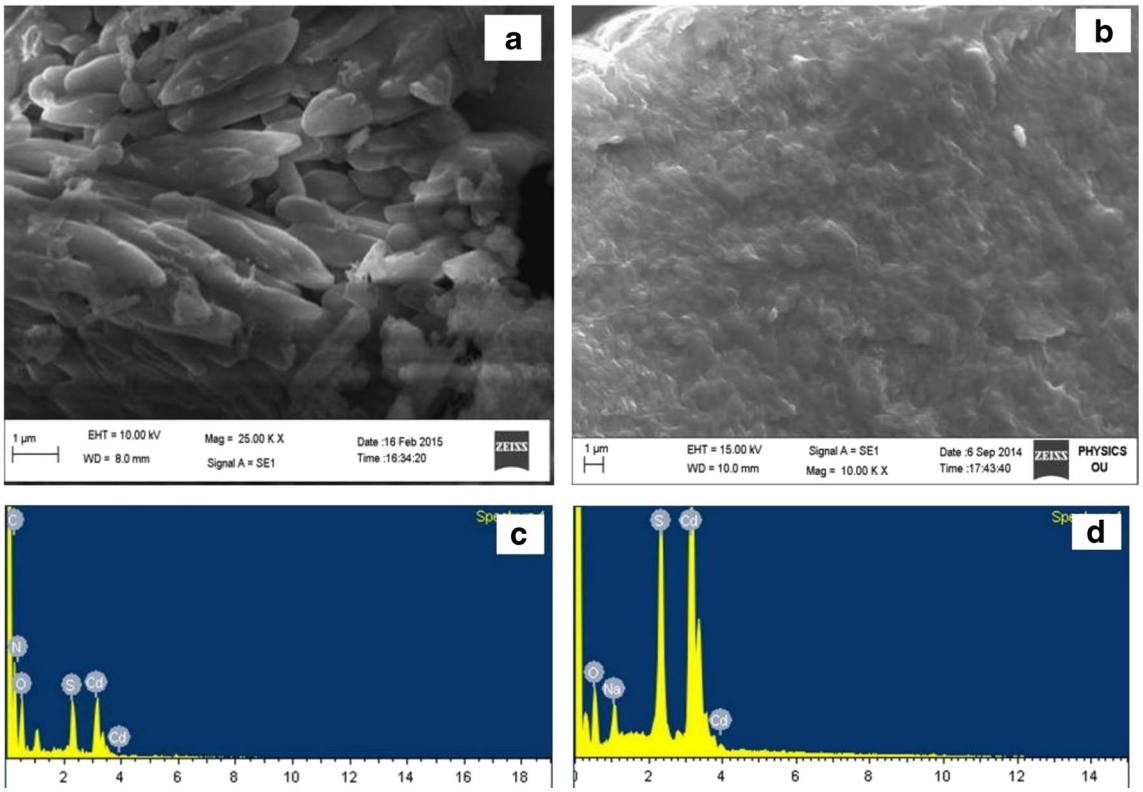

Fig. 4 **a**–**b** SEM micrographs of SB capped and uncapped CdS NPs **c**–**d** corresponding EDX images

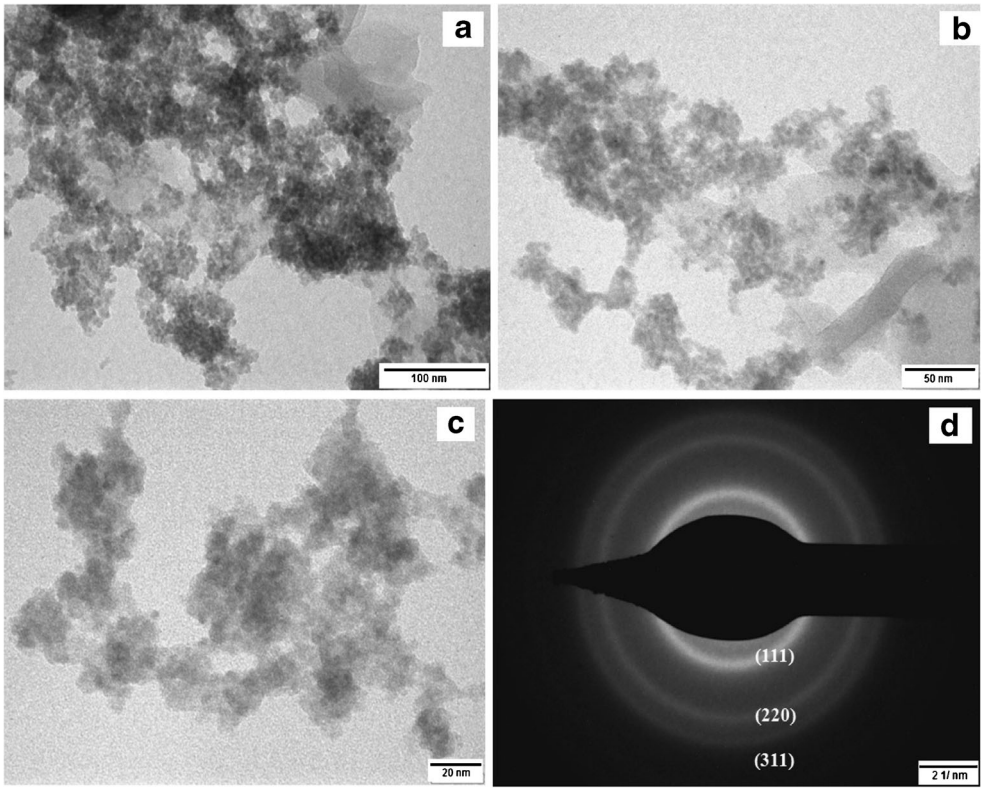

Fig. 5 The TEM images of **a** 100 nm, **b** 50 nm, **c** 20 nm magnifications and **d** corresponding SAED pattern of CdS NPs

CdS NPs was about 590 nm, corresponding to a band gap of 2.10 eV, which was smaller than the reported in literature (CdS, 2.42 eV) [31]. The band gap of the material can be estimated by using the formula: $E_g=1240/\lambda$, where E_g is the band gap energy and λ is the wavelength of the absorption edge. A blue shift was observed for the uncapped and SB capped CdS NPS, the absorption edge shifted to 576 nm (2.14 eV) and 570 nm (2.17 eV) respectively. It may be due to the size quantization effect, the grain size decrease leads to the energy gap wider and a blue shift was found [32].

FTIR Analysis

Figure 2 shows the FTIR spectrum of synthesized CdS NPs at room temperature in the range of 4000–250 cm^{-1}. In the FTIR spectrum of SB capped CdS NPs, the strong absorption peaks at 3435 cm^{-1}, 1556 cm^{-1}, 1412 cm^{-1}, 1330 cm^{-1} and 1016 cm^{-1} are assigned to O-H stretching in phenols, N = O stretching in nitro compounds, C-C stretching in aromatics, C-N stretching and C-O stretching respectively. For the SB capped CdS NPs, when compared to SB, the increase in the intensity is followed by the shifting of the peaks are observed in all the cases. The new weak bands observed at 674, 582 and 481 cm^{-1} which are not seen in the spectrum of SB can be attributed to υ(Cd–O), υ(Cd–N) and υ(Cd-S). This also testifies the interaction of Cd with SB, in other words, CdS NPs are modified by SB. In uncapped CdS NPs, the strong absorption peaks observed at 3427, 1562, 1412, 1009 and 672 cm^{-1} are attributed to form CdS NPs.

XRD Analysis

The structural analysis of the synthesized CdS NPs has been carried out using XRD. The XRD pattern in Fig. 3 consists of three diffraction peaks located at 2 =26.1^0, 43.8^0 and 51.5^0

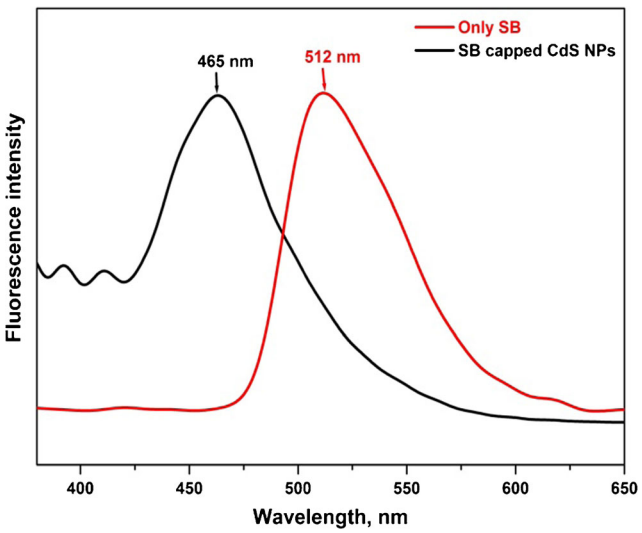

Fig. 6 The fluorescence emission spectra of SB and SB capped CdS NPs

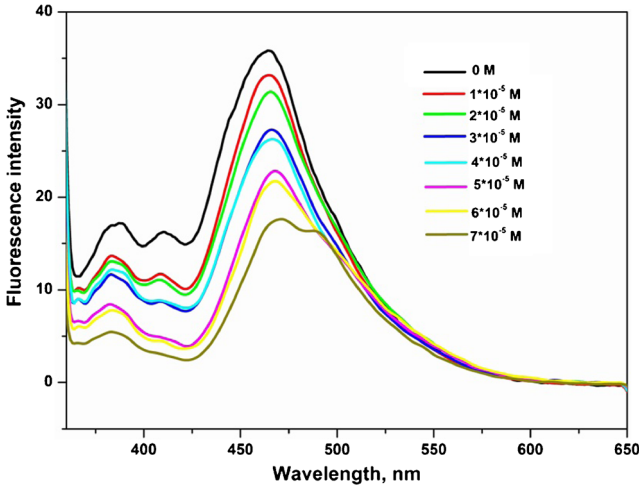

Fig. 7 Fluorescence spectra of CdS NPs quenched by SB in the concentration range of $0–7\times10^{-5}$ M

which can also be indexed as (111), (220) and (311) crystallographic planes, respectively, indicating again that, as-prepared CdS NPs belong to the face-centred cubic phase with the zinc blende structure. The particle size of CdS NPs was estimated based on the full width at half-maximum (FWHM) of the (111) peak according to the Debye-Scherrer equation shown as follows:

$$D = \frac{K\lambda}{\beta\cos\theta}$$

Where K is a constant (shape factor, about 0.89), λ is the X-ray wavelength, β is the FWHM of the diffraction line, and is the diffraction angle. It can be observed that the average particle sizes were in the range of 5–15 nm based on (111) crystal plane. The lattice parameters of SB capped and uncapped CdS NPs found to be 5.98 and 5.79 A^{o} respectively.

SEM & EDX Study

SEM is a suitable technique for study of the morphology of materials. SEM micrograph with EDX spectra recorded for CdS NPs are shown in Fig. 4a–d. From the SEM image it is noticed that the surface morphology is in the form of assemblies of nanoparticles having different shapes. The chemical composition of CdS NPs was measured through the EDX spectrum. According to EDX, the particles consist of O, C, N, Cd and S. The peaks of C, N and O were mainly generated by SB and the peaks of Cd and S were generated by CdS NPs.

TEM Study

Figure 5a–c shows the typical TEM image of prepared SB capped CdS NPs at room temperature. NPs exhibit monodispersity and nearly spherical shape with a narrow size distribution. The average particle size is in the range of 2–10 nm. The selected area electron diffraction (SAED, Fig. 5d) clearly gives three diffraction rings of (111), (220) and (311) planes from inner to outer, respectively, which identifies the cubic phase. Some nanoparticles get aggregated due to large specific surface area and high surface energy. The aggregation occurred probably during the process of drying.

Electrophoretic Light Scattering Study

The variation in zeta potential of uncapped and SB capped CdS NPs in their aqueous dispersion was recorded. The observed value of ζ, -2.04 and 2.98 mV for uncapped and SB capped CdS NPs respectively reveal that their aqueous suspensions are quite stable because of the electrostatic repulsions between the same charged species. When CdS NPs dispersed in water then the surface becomes anionic in nature and

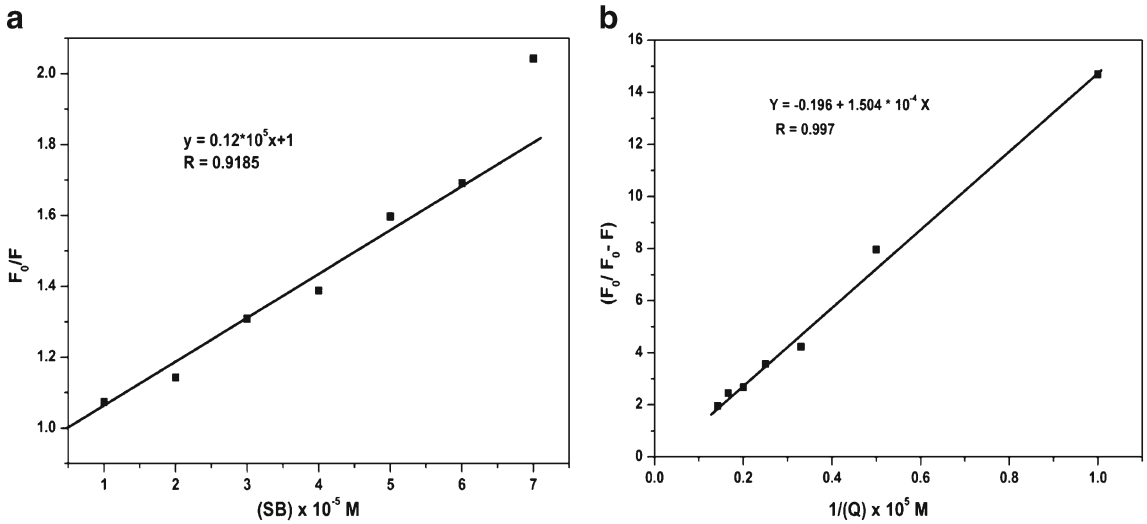

Fig. 8 **a** Stern-Volmer plot and **b** modified stern-Volmer plot of CdS NPs in presence of SB

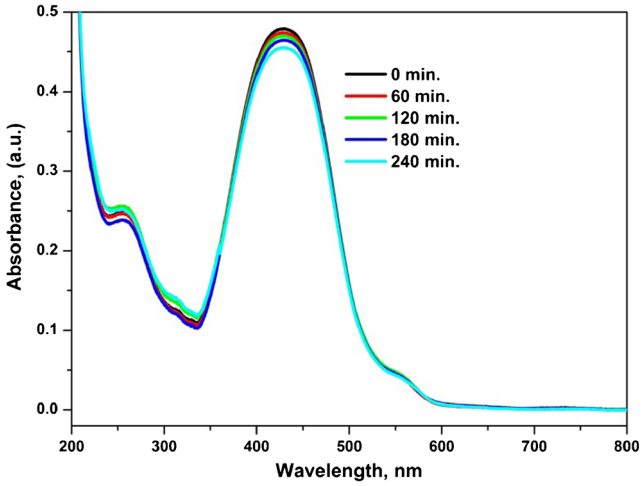

Fig. 9 Photocatalytic degradation of MR dye in the absence of catalyst under sunlight irradiation

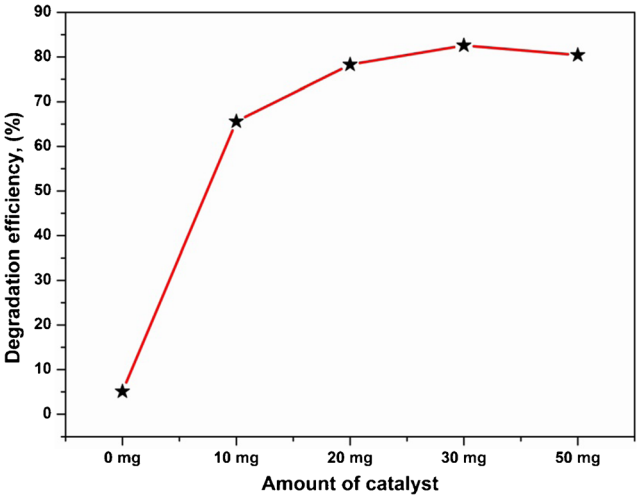

Fig. 11 The variation of degradation efficiency with amount of catalyst

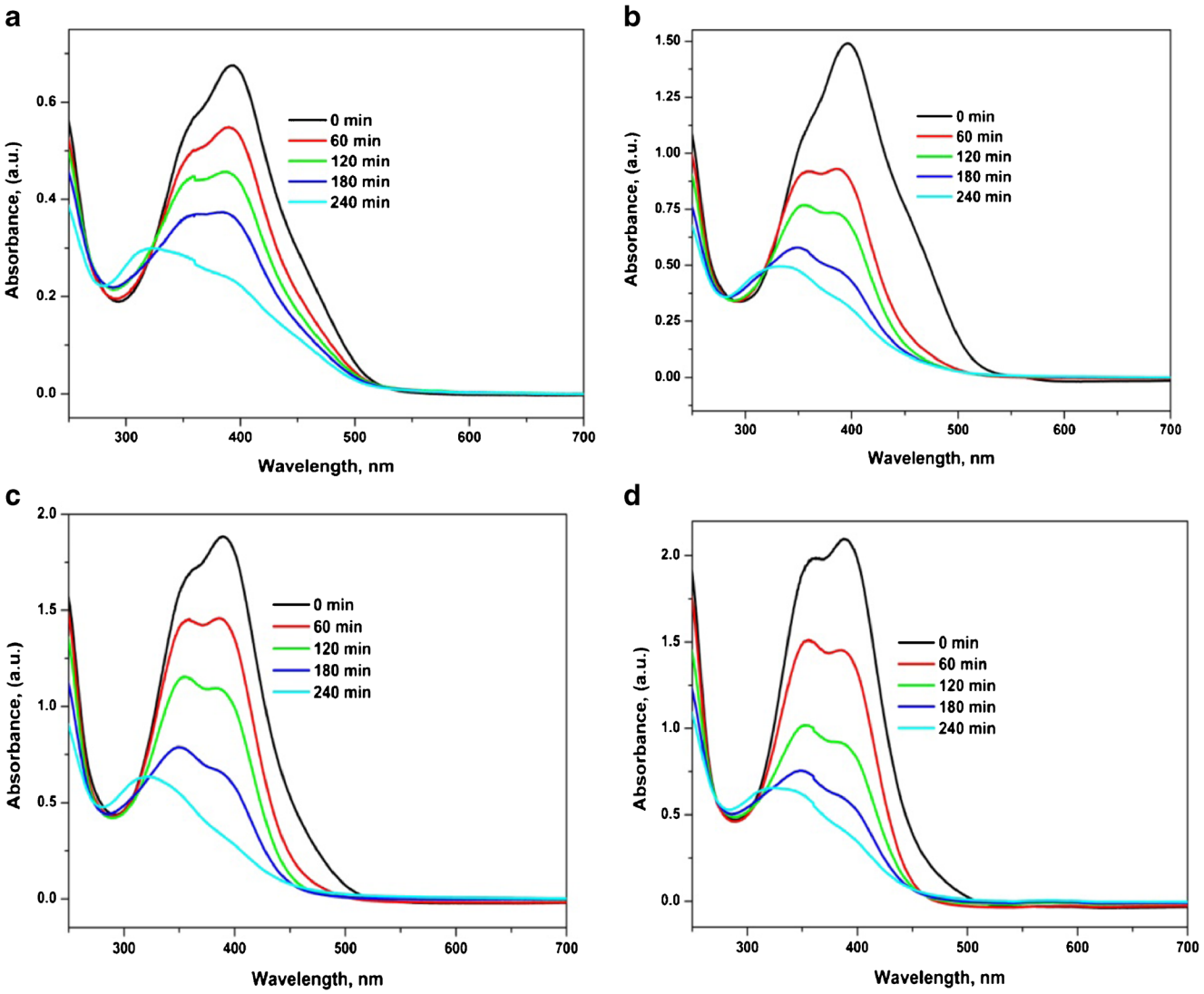

Fig. 10 Photocatalytic degradation of MR dye using **a** 10 mg, **b** 20 mg, **c** 30 mg and **d** 50 mg of catalyst under sunlight irradiation

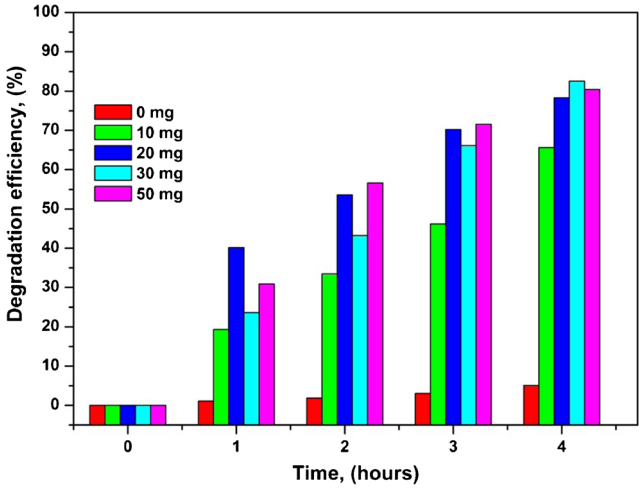

Fig. 12 The percentage of degradation efficiency of MR dye under sunlight irradiation

the surface area increases that would render the more coverage of hydroxyl groups from water [33].

Fluorescence Study

Fluorescence Measurement

Fluorescence spectra (Fig. 6) indicate that the SB and SB capped CdS NPs exhibited emission peaks with slightly different full-width-at-half-maximum (FWHM) values of 58 nm (SB), 46 nm (SB-CdS NPs). Emission maximum of SB was found to be at around 512 nm (2.41 eV), while that of SB capped CdS NPs was shifted to around 465 nm (2.65 eV). The fluorescence emission spectra of the CdS NPs solutions showed a significant bathochromic shift of the emission maxima by complexation of SB, in comparison with fluorescence of SB. It is well known that the size of the nanoparticles is related to their absorption maximum and the surface quality is related to their fluorescence emission.

Fluorescence Interaction Studies of CdS NPs with SB

The fluorescence interaction spectra of CdS NPs in the presence of SB are shown in Fig. 7. The fluorescence intensity of CdS NPs was significantly decreased without any change in the emission maximum and spectral shape as the concentration of SB was increased, this suggests that the SB quenched the fluorescence effectively [34]. Sonochemically synthesized SB capped CdS NPs and SB were soluble in DMF. The SB solutions of $1–7\times10^{-5}$ M concentrations are prepared in DMF and subsequently were added to the 2×10^{-5} M CdS NPs solution. Then the fluorescence intensity of mixed solutions was measured. The fluorescence band of CdS NPs at 465 nm gradually decreased from a concentration of 1×10^{-5} M and vanished when 7×10^{-5} M SB was added, which may probably be due to a stronger interaction between SB and CdS NPs. The normalized quenching intensities (F/F_0; F and F_0 is the fluorescence intensities of CdS NPs in the presence and absence of the SB, respectively) versus concentration of SB suggests that it quenches CdS NPs more efficiently. To analyze the dependence of the fluorescence intensity on the SB concentration, Stern–Volmer relationship has been used.

$$\frac{Fo}{F} = 1 + Ksv[Q]$$

Where, K_{SV} is the Stern–Volmer constant which is a measure of the efficiency of quenching and [Q] is the concentration of the SB [35]. By plotting (F_0/F) versus [Q], K_{SV} can be calculated from the slopes of the linear Stern–Volmer plots. In Fig. 8a, the Stern–Volmer plot of CdS NPs was shown. From the slope of the linear plot, the Stern–Volmer quenching constant K_{SV} (0.12×10^5 L mol^{-1}) was calculated. The results of the fluorescence study indicated that the quenching effect of SB on the fluorescence emission of CdS NPs is found to be

Scheme 2 The possible degradation mechanism of MR dye using ESI-MS

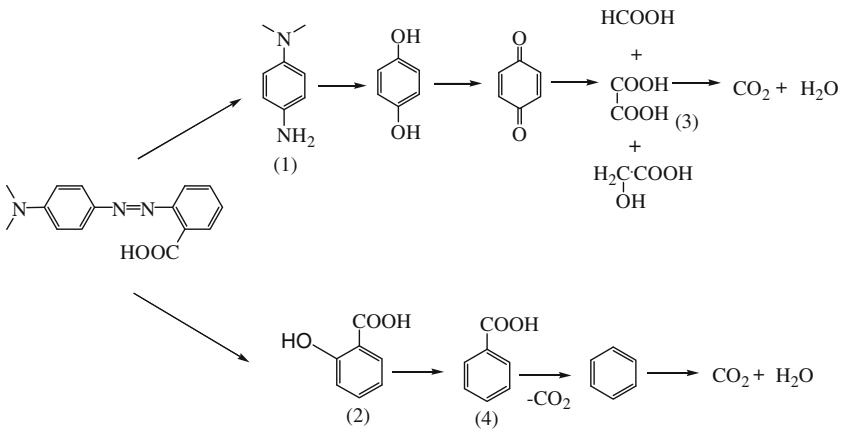

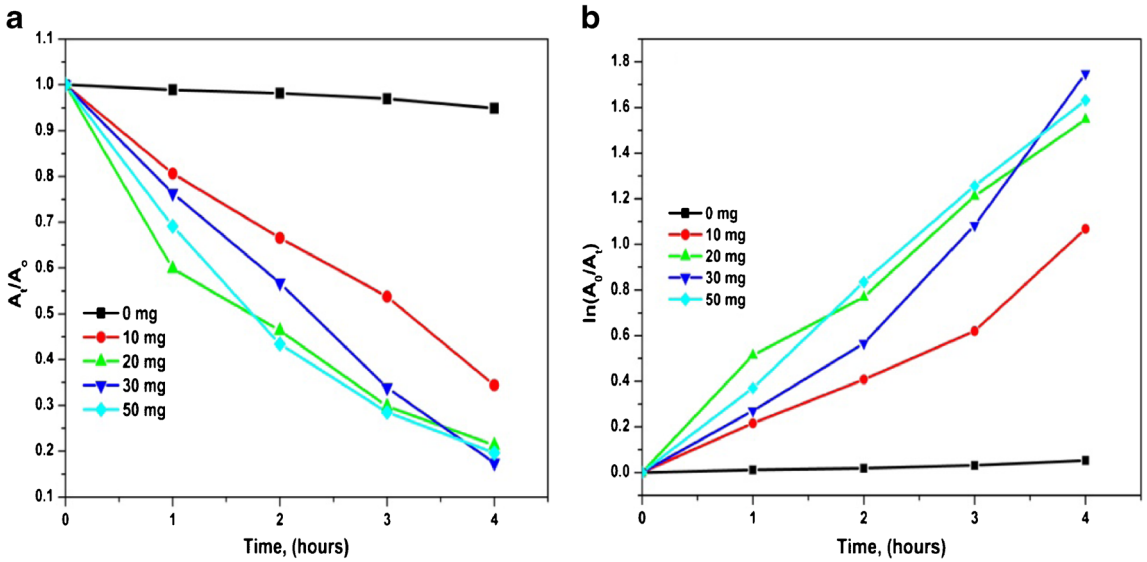

Fig. 13 **a** A_t/A_o curves and **b** kinetic plots for photocatalytic degradation of MR under sunlight irradiation

concentration dependent. The quenching data was analyzed according to the modified Stern–Volmer equation:

$$\frac{Fo}{Fo-F} = \frac{1}{fa\,ka}\frac{1}{[Q]} + \frac{1}{fa}$$

Where, f_a is the fraction of the initial fluorescence and K_a is the effective quenching constant. A plot of $(F_0-F)/F$ versus 1/[Q] (Fig. 8b) gives a straight line where the values of K_a of CdS NPs has been found to be $0.13\times10^4\ M^{-1}$, from slope and f_a was found to be 5.102 from intercept of the plot.

Photocatalytic Degradation Study

The photocatalytic degradation of MR was studied in the presence of varying amounts of CdS NPs. The position of absorption wavelength changes in the optical absorption spectrum to 394 nm in the presence of CdS NPs. The reaction vessel was exposed to sunlight irradiation for 4 h in the absence of CdS NPs. Only a very small change in the intensity of the maximum absorption was observed after 4 h irradiation in the absence of CdS NPs and the UV-vis absorption spectra was shown in Fig. 9. The effect of amount of catalyst on the degradation of MR was investigated systematically under sunlight irradiation.

Figure 10a–d shows the absorption spectra of MR after addition of 10, 20, 30 and 50 mg of catalyst under sunlight irradiation. The intensity of the peak decreases with increase in irradiation time due to photocatalytic degradation of MR. It indicates that the photocatalytic efficiency in the presence of CdS NPs was higher than in the absence of catalyst. It was observed that there is an enhancement of photocatalytic degradation efficiency of MR dye with the 30 mg of catalyst among 10, 20, 30 and 50 mg of catalyst (Fig. 11). The rate of MR degradation was found to be faster in 30 mg amount of catalyst. Moreover, the photocatalytic activity of a photocatalyst depends on the amount of catalyst and its percentage content on the surface of the catalyst. The amount of catalyst is also likely to affect the rate of dye bleaching and hence photocatalytic bleaching was observed using different amounts of photocatalyst. The degradation efficiencies in the absence and presence of various amounts catalyst were calculated in photodegradation of MR dye. Figure 12 shows the detailed photocatalytic degradation efficiency of MR dye in the absence and presence of CdS NPs with increasing reaction irradiation time under solar irradiations. Finally, the

Table 1 The calculated values of degradation efficiency and rate constants of photo degradation of MR dye

S. no	Amount of catalyst	% of degradation	Rateconstant, k (min^{-1})	R^2
1	0 mg	5.07	0.012	0.98
2	10 mg	65.61	0.254	0.98
3	20 mg	78.29	0.379	0.99
4	30 mg	82.59	0.431	0.98
5	50 mg	80.43	0.415	0.99

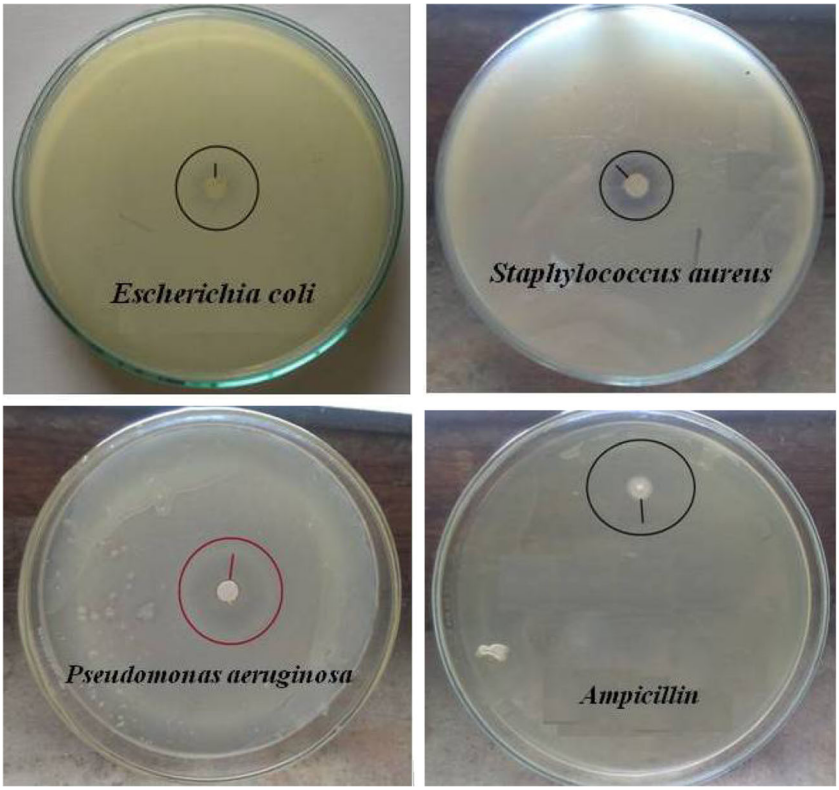

Fig. 14 Antibacterial test results of *E. coli*, *S. aureus* and *P. aeruginosa* after 24 h incubation by SB capped CdS NPs. Ampicillin used as positive control

significant photocatalytic performance of the CdS NPs was observed with the commercially available Degussa P25 and TiO_2. The superior performance of Degussa P25 over TiO_2 samples of a different origin has often been reported in the literature with a number of postulations being suggested in order to explain its high photo activity, with regards to both its surface and bulk properties [36–41].

Degradation Mechanism of MR dye

The degradation mechanism of MR was carried out by the ESI-MS analysis. The degradation products may be more harmful and persistent than the parent compound [42]. Therefore, it is necessary to identify the degradation products. The mass spectrum recorded at the time of decolorisation of the dye for this process shows m/z peaks at 136 and 138 attributed to the formation of 4,4-N,N-dimethyl aniline (1) and 2-hydroxy benzoic acid (2). Based on the intermediates obtained, probable degradation mechanisms have been proposed in Scheme 2. The intermediates (1 and 2) are formed on the CdS NPs surface due to the attack of hydroxyl radicals at the site of the azo bond. During irradiation the degradation products of intermediate (1) proceeds through the formation of hydroxylated aromatic derivatives like 1, 4-dihydroxy benzene and hydroquinone. After 2 h of irradiation mass spectrum shows corresponding peaks, which were due to the formation of simple aliphatic carboxylic acids like oxalic acid (3), formic acid and glyoxalic acid. Ring opening reaction of hydroquinone results in the formation of the above intermediates. The intermediate (2) further undergoes to formation of benzoic acid (4). After 4 h of solar irradiation, the mass spectrum showed no characteristic peaks belonging to any functional group confirming the complete mineralization of the dye.

Kinetic Studies of Photocatalytic Degradation of MR

The Langmuir-Hinshelwood method can be used to describe the rates of the photocatalytic degradation of MR in the

Table 2 Zone of inhibition study on *E. coli, S. aureus* and *P. aeruginosa* bacterias with prepared samples against ampicillin (control)

S. no	Sample	Zone of inhibition in mm			
		E.coli	*S.aureus*	*P.aeruginosa*	Ampicillin
1	SB capped CdS NPs	18.04	21.31	25.6	27.4
2	Uncapped CdS NPs	6.09	7.62	10.92	26.6
3	SB	18.11	17.27	20.02	27.1

presence of CdS NPs as a function of irradiation time [43]. The ratio of absorbances with increasing reaction irradiation time and initial absorbance (A_t/A_o) was plotted against irradiation time as shown in Fig. 13a. It shows a gradual decrease with reaction time. Plotting the natural logarithm of the ratio between the original absorbance of MR and the absorbance after photocatalytic degradation [$\ln(A_o/A_t)$] against the irradiation time yields a linear relationship as shown in Fig. 13b. Therefore, the photocatalytic degradation reaction of MR by CdS NPs follows the pseudo-first order reaction kinetics. The adsorption rate constant and degradation efficiency values of MR with amount of SB capped CdS NPs under sunlight irradiation are summarised in Table 1.

Antibacterial Activity Study

The details of the antibacterial experiment were provided in the experimental section. In present study antibacterial activities of prepared samples were tested by paper disc method using *E. coli, S. aureus* and *P. aeruginosa* and shown in Fig. 14. The SB and CdS NPs are very promising in exhibiting their ability to inhibit/destroy both gram positive and gram negative pathogenic bacteria. The zone of inhibition was measured for uncapped and SB capped CdS NPs as well as SB against the bacteria *E. coli, S. aureus* and *P. aeruginosa* at 1 mg/ml concentration by the paper disc method using nutrient agar as the medium and shown in Table 2. An increase in the lipophilic character of the complex favours its permeation through the lipid layer of the bacterial membrane, and therefore shows higher activity. The higher activity of the complexes compared to free ligand may be attributed to chelation [44] which reduces polarity of the metal ion by partial sharing of the positive charge with donor atoms of the ligand. This increases the lipophilic character, favouring the permeation through lipid layers of the bacterial membrane. The SB can penetrate the bacterial cell membrane by coordination of metal ion through oxygen or nitrogen donor atom to lipopolysaccharide which leads to the damage of outer cell membrane and consequently inhibits the growth of the bacteria. Therefore, the SB capped CdS NPs exhibited more antibacterial activity against all bacteria than with SB or CdS NPs alone.

Conclusions

The CdS NPs were successfully synthesized by a sonochemical method using SB as a complexing agent. The results obtained in the present study show that the sonochemical method has proved to be simple and impressive. The use of toxic chemicals and time-consuming methods can be avoided by using this method. This method brings forward a broad idea to synthesize other metal sulfides with various morphologies and novel properties. The interactions among CdS NPs and SB were investigated using fluorescence studies. The study of fluorescence of CdS NPS with the increasing SB concentration indicates some static fluorescence quenching seems to be involved in the quenching mechanism. Synthesized NPs have been used for photocatalytic degradation of MR under sunlight irradiation. The results of this study prove that the amount of catalyst and sunlight are significantly affects the photocatalytic degradation of dye. The Langmuir-Hinshelwood kinetic analyses revealed that pseudo-first order kinetics is followed for the degradation of dye. The prepared samples were screened for their antibacterial activity against bacteria. The results showed that the SB capped CdS NPs are biologically active.

Acknowledgments The authors would like to acknowledge Head, Department of Chemistry, Osmania University for providing necessary facilities. One of the authors, D. Ayodhya wishes to thank the UGC, New Delhi for award of SRF which supported this work.

References

1. Alivisatos AP (1996) Semiconductor clusters, nanocrystals, and quantum dots. Science 271:933–937. doi:10.1126/science.271.5251.933
2. Yu WW, Peng X (2002) Formation of high-quality CdS and other II-VI semiconductor nanocrystals in noncoordinating solvents: tunable reactivity of monomers. Angew Chem Int Ed 41:2368–2371
3. Jie JS, Zhang WJ, Jiang Y, Meng XM, Li YQ, Lee ST (2006) Photoconductive characteristics of single-crystal CdS nanoribbons. Nano Lett 6:1887–1892. doi:10.1021/nl060867g
4. Qingqing W, Gang X, Gaorong H (2005) Solvothermal synthesis and characterization of uniform CdS nanowires in high yield. J Solid State Chem 178:2680–2685. doi:10.1016/j.jssc.2005.06.005
5. Ma X, Xu F, Liu Y, Liu X, Zhang Z, Qian Y (2005) Double-dentate solvent-directed growth of multi-armed CdS nanorod-based semiconductors. Mater Res Bull 40:2180–2188. doi:10.1016/j.materresbull.2005.07.009
6. Wang Y, To CY, Ng DHL (2006) Controlled synthesis of CdS nanobelts and the study of their cathodoluminescence. Mater Lett 60:1151–1155. doi:10.1016/j.matlet.2005.10.098
7. Murugan AV, Sonawane RS, Kale BB, Apte SK, Kulkarni AV (2001) Microwave–solvothermal synthesis of nanocrystalline cadmium sulfide. Mater Chem Phys 71:98–102
8. Kristl M, Ban I, Danc A, Danc V, Drofenik M (2010) A sonochemical method for the preparation of cadmium sulfide and cadmium selenide nanoparticles in aqueous solutions. Ultrason Sonochem 17:916–922. doi:10.1016/j.ultsonch.2009.12.013
9. Bao C, Jin M, Lu R, Xue P, Zhang Q, Wang D, Zhao Y (2003) Surfactant–ligand co-assisted solvothermal technique for the synthesis of different-shaped CdS nanorod-based materials. J Solid State Chem 175:322–327. doi:10.1016/S0022-4596(03)00298-6
10. Pol VG, Palchik O, Gedanken A, Felner I (2002) Synthesis of europium oxide nanorods by ultrasound irradiation. J Phys Chem B 106:9737–9743. doi:10.1021/jp025864g
11. Gates B, Mayers B, Grossman A, Xia Y (2002) A sonochemical approach to the synthesis of crystalline selenium nanowires in solutions and on solid supports. Adv Mater 14:1749–1752
12. Katoh R, Tasaka Y, Sekreta E, Yumura M, Ikazaki F, Kakudate Y, Fujiwara S (1999) Sonochemical production of a carbon nanotube. Ultrason Sonochem 6:185–187

13. Wang H, Lu YN, Zhu JJ, Chen HY (2003) Sonochemical fabrication and characterization of stibnite nanorods. Inorg Chem 42: 6404–6411. doi:10.1021/ic0342604
14. Niasari MS, Hosseinzadeh G, Davar F (2011) Synthesis of lanthanum carbonate nanoparticles via sonochemical method for preparation of lanthanum hydroxide and lanthanum oxide nanoparticles. J Alloys Compd 509:134–140. doi:10.1016/j.jallcom.2010.09.006
15. Buitron G, Quezada M, Moreno G (2004) Aerobic degradation of the azo dye acid red 151 in a sequencing batch bio-filter. Bioresour Technol 92:143–149. doi:10.1016/j.biortech.2003.09.001
16. Sokmen M, Allen DW, Akkas F, Kartal N, Acar F (2001) Photodegradation of some dyes using Ag-loaded titanium dioxide. Water Air Soil Pollut 132:153–163
17. Sauer T, Neto GC, Jose HJ, Moreira RFPM (2002) Kinetics of photocatalytic degradation of reactive dyes in a TiO_2 slurry reactor. J Photochem Photobiol A Chem 149:147–154
18. Rajeshwar K, Osugi ME, Chanmanee W, Chenthamarakshan CR, Zanoni MVB, Kajitvichyanukul P, Ayer RK (2008) Heterogeneous photocatalytic treatment of organic dyes in air and aqueous media. J Photochem Photobiol C 9:171–192. doi:10.1016/j.jphotochemrev.2008.09.001
19. Lachheb H, Puzenat E, Houas A, Ksibi M, Elaloui E, Guillard C, Herrmann JM (2002) Photocatalytic degradation of various types of dyes (Alizarin S, Crocein Orange G, Methyl Red, Congo Red, Methylene Blue) in water by UV-irradiated titania. Appl Catal B Environ 39:75–90. doi:10.1016/S0926-3373(02)00078-4
20. Guindo MC, Zurita L, Duran JDG, Delgado AV (1996) Electrokinetic behavior of spherical colloidal particles of cadmium sulfide. Mater Chem Phys 44:51–58
21. Matijevic E, Wilhelmy DM (1982) Preparation and properties of monodispersed spherical colloidal particles of cadmium sulfide. J Colloid Interface Sci 86:476–484. doi:10.1016/0021-9797(82)90093-5
22. Alivisatos AP (1996) Perspectives on the physical chemistry of semiconductor nanocrystals. J Phys Chem 100:13226–13239
23. Burda C, Chen X, Narayanan R, El-Sayed MA (2005) Chemistry and properties of nanocrystals of different shapes. Chem Rev 105: 1025–1102. doi:10.1021/cr030063a
24. Smith AM, Nie S (2004) Chemical analysis and cellular imaging with quantum dots. Analyst 129:672–677
25. Sharma P, Brown S, Walter G, Santra S, Moudgil B (2006) Nanoparticles for bioimaging. Adv Colloid Interface Sci 123: 471–485. doi:10.1016/j.cis.2006.05.026
26. Wu CL, Zhao YB (2007) CdS quantum dots as fluorescence probes for the sensitive and selective detection of highly reactive HSe^- ions in aqueous solution. Anal Bioanal Chem 388:717–722. doi:10.1007/s00216-007-1246-7
27. Chen JL, Zhu CQ (2005) Functionalized cadmium sulfide quantum dots as fluorescence probe for silver ion determination. Anal Chim Acta 546:147–153. doi:10.1016/j.aca.2005.05.006
28. Gaballa AS, Asker MS, Barakat AS, Teleb SM (2007) Synthesis, characterization and biological activity of some platinum (II) complexes with Schiff bases derived from salicylaldehyde, 2-furaldehyde and phenylenediamine. Specrochim Acta A 67:114–121. doi:10.1016/j.saa.2006.06.031
29. Shi L, Ge HM, Tan SH, Li HQ, Song YC, Zhu HL, Tan RX (2007) Synthesis and antimicrobial activities of Schiff bases derived from 5-chloro-salicylaldehyde. Eur J Med Chem 42:558–564. doi:10.1016/j.ejmech.2006.11.010
30. Isin K, Erbil A, Ferda E, Samil I (2009) 2-[(4-Methoxyphenyl)iminomethyl]-4-nitrophenol. Acta Crystallogr E 65:0737. doi:10.1107/S1600536809008150
31. Hu Y, Liu Y, Qian H, Li Z, Chen J (2010) Coating colloidal carbon spheres with CdS Nanoparticles: microwave-assisted synthesis and enhanced photocatalytic activity. Langmuir 26:18570–18575. doi:10.1021/la103191y
32. Liu B, Lee JY (2005) Ordered alignment of CdS nanocrystals on MWCNTs without surface modification. J Phys Chem B 109: 23783–23786. doi:10.1021/jp056196c
33. Sahu M, Biswas P (2011) Single-step processing of copper-doped titania nanomaterials in a flame aerosol reactor. Nanoscale Res Lett 6:441–455
34. Koneswaran M, Narayanaswamy R (2009) Mercaptoacetic acid capped CdS quantum dots as fluorescence single shot probe for mercury (II). Sensors Actuators B 139:91–96. doi:10.1016/j.snb.2008.09.011
35. Valeur B (2002) Molecular fluorescence: principles and applications, 1st edn. Wiley-VCH Verlag GmbH, Wenham
36. Navio JA, Testa JJ, Djedjeian P, Padron JR, Rodriguez D, Litter MI (1999) Iron-doped titania powders prepared by a sol–gel method.: part II: photocatalytic properties. Appl Catal Gen 178:191–203. doi:10.1016/S0926-860X(98)00286-5
37. Hoffmann MR, Martin ST, Choi W, Bahnemann DW (1995) Environmental applications of semiconductor photocatalysis. Chem Rev 95:69–96
38. Preis S, Krichevskaya M, Terentyeva J (1999) Treatment of phenolic and aromatic amino compounds by photocatalytical oxidation in polluted waters. TiO2-4: The Fourth International Conference on TiO2 Photocatalytic Purification and Treatment of Water and Air, Albuquerque
39. Martin S, Herrmann H, Choi W, Hoffmann ZM (1995) Photochemical destruction of chemical contaminants on quantum sized semiconductor particles. Solar Eng ASME 1:409–413
40. Lepore GP, Langford CH, Vichova J, Vlcek A (1993) Photochemistry and picosecond absorption spectra of aqueous suspensions of a polycrystalline titanium dioxide optically transparent in the visible spectrum. J Photochem Photobio A Chem 75:67–75. doi:10.1016/1010-6030(93)80161-2
41. Zhang Z, Wang C, Zakaria R, Ying JY (1998) Role of particle size in nanocrystalline TiO2-based photocatalysts. J Phys Chem B 102: 10871–10878
42. Sanchez-Prado L, Llompart M, Lores M, Garcia-Jares C, Bayona JM, Cela R (2006) Monitoring the photochemical degradation of triclosan in waste water by UV light and sunlight using solid-phase microextraction. Chemosphere 65:1338–1347. doi:10.1016/j.chemosphere.2006.04.025
43. Houas A, Lachheb H, Ksibi M, Elaloui E, Guillard C, Herrmann JM (2001) Photocatalytic degradation pathway of methylene blue in water. Appl Catal B Environ 31:145–157
44. Osowole AA, Kolawole GA, Fagade OE (2008) Synthesis, characterization and biological studies on unsymmetrical Schiff-base complexes of nickel(II), copper(II) and zinc(II) and adducts with 2,2′-dipyridine and 1,10-phenanthroline. J Coord Chem 61:1046–1055. doi:10.1080/00958970701482446